Chapter 7

Measurements

In this chapter the first experimental results obtained with the spectrometer are presented. In the first section, the calibration of the magnetic field axis utilizing the $^{55}Mn^{2+}$ standard will be described. The following section deals with the suitability of DPPH as a standard for high–field measurements. Typical features of the powder patterns of nitroxide radicals are highlighted in section 7.2. The enhancement of the spectral resolution at 360 GHz measurement frequency compared to W–band EPR is demonstrated in section 7.3. In the last section, measurements of spin–labeled bacteriorhodopsin are presented.

7.1 Magnetic field calibration

To determine absolute values for the g–factor of a sample, two approaches can be taken. One is to directly measure the B–field and the microwave frequency. This usually is the method of choice in lower frequency (below W–band) EPR measurements. Under high–field / high–frequency conditions, several factors come into play that render this method difficult, if not impossible: The superconducting magnets at high fields do not allow to sweep the magnetic field with sufficiently high linearity. This makes it impossible

to simply determine the field values at the start and end of a sweep and then interpolate. Even more importantly, the determination of an absolute field value by measurement of the current in the superconducting coils is extremely inaccurate and dependent on factors such as sweep rate and direction (see figure 5.13).

The second approach consists of placing a standard sample with well known spectroscopic parameters in the resonator together with the sample under investigation. A standard sample has to meet several requirements: Its spectral parameters (g–factor, fine and hyperfine constants) have to be known with sufficiently high precision. In addition, its spectrum should be spread over a wide enough frequency range compared to the spectra to be investigated, in order to provide a sufficient number of reference points for broad spectra. Further requirements are a high chemical stability and a narrow line width to avoid excessive overlap of the spectra of sample and standard as well as to allow for a precise determination of the line position.

7.1.1 The $^{55}Mn^{2+}$ standard

The standard sample used in the W–band spectrometer of our work group (Burghaus et al. 1992) is the $^{55}Mn^{2+}$ ion in MnO/MgO polycrystalline powder. It has an electron spin $S = \frac{5}{2}$ and a nuclear spin $I = \frac{5}{2}$ and therefore 30 allowed transitions with $\Delta M_S = \pm 1$ and $\Delta M_I = 0$.

The resonance field positions for these transitions can be obtained from second order perturbation theory to (W. Low 1957):

$$B = B_0 - AM_I - \frac{A^2}{2B_0}\left[I\,(I+1) - M_I^2 + M_I(2M_S - 1)\right] \qquad (7.1)$$
$$+ \text{ higher order terms}$$

At a central magnetic field of $B_0 = 12.85$ T, its spectrum consists of 6 narrow lines with a linewidth of 0.1 mT that are spread over a field range of 45 mT (figure 7.1). While in principle each of these lines consists of 5

transitions that are separated by the second order term in equation 7.1, this term becomes almost negligible for high magnetic fields. Moreover, the transitions for $M_S = \pm\frac{5}{2} \leftrightarrow \pm\frac{3}{2}$ and $M_S = \pm\frac{3}{2} \leftrightarrow \pm\frac{1}{2}$ are extremely broadened due to the electron–electron dipolar zero field splitting and thus cannot be detected. The only transition to be observed therefore is the $M_S = \pm\frac{1}{2} \leftrightarrow \pm\frac{1}{2}$ transition.

The values for the isotropic g–factor and the isotropic hyperfine coupling constant have been measured in X–band to high precision (Burghaus et al.

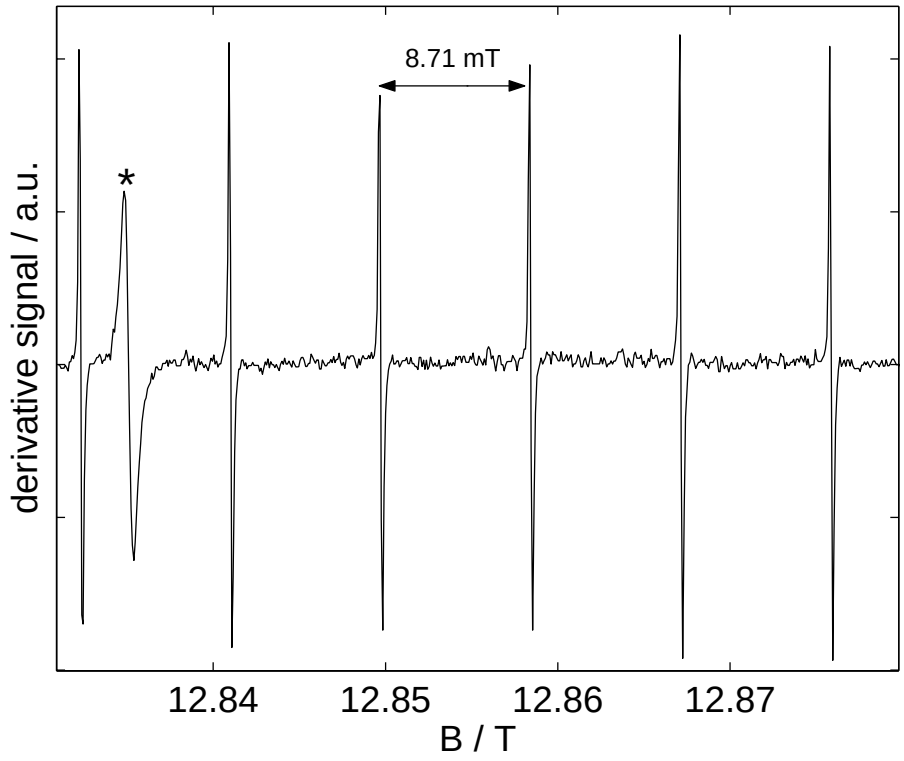

Figure 7.1: EPR spectrum of Mn^{2+} / MgO 0.01 % polycrystalline powder at 360 GHz. The line marked with (*) is a signal due to free radicals in a rest of coal that originates from the synthesis process.

1992):

$$\begin{aligned} g_{\mathrm{Mn}^{2+}} &= 2.00101 \pm 0.00005 \\ A_{\mathrm{Mn}^{2+}} &= -(8.710 \pm 0.003)\ \mathrm{mT} \end{aligned}$$

In summary, the Mn^{2+} standard provides 6 reference points in the measured spectra. Under the assumption of a perfectly linear magnetic field sweep, two lines would suffice to calibrate the B–axis. In our measurements, however, it turned out that the sweep field is not entirely linear with the sweep current, i.e. the magnetic field lags the current through the coils in dependence of the sweep rate and the sweep direction. For spectra that lie within the range of the Mn^{2+} lines, it is then possible to interpolate the B–axis between successive lines.

For this purpose, an algorithm was developed that took the field sweep current values I_i of 3 or more of the lines as an input and performed a best fit to a function $B(I)$ where $B(I)$ was a 3rd order polynomial. The fit criterion was to minimize the squared deviation of the values $B(I_i)$ from the true resonance field positions of the respective Mn^{2+} lines. To estimate the margin of error of g–values obtained by this calibration of the field axis, the uncertainty in the position of the Mn lines was determined from plots of several different spectra. The observed uncertainty in field values, even for a very conservative assumption for the line position uncertainty, does not lead to errors in g–values greater than ± 0.00002. Therefore, the error for absolute g–values that are obtained from field positions that lie within the range of the Mn hyperfine spectrum is taken to be that of the Mn field standard itself, ± 0.00005.

The situation is entirely different for spectral features that lie to the low– or high–field side of the Mn lines. There, the field calibration procedure is an extrapolation, rather than an interpolation. The nonlinear interpolation procedure then can produce rather large errors depending on how far the

extrapolation has to reach. In the case of the g_{xx}–values of the nitroxide radicals presented later in this chapter, under the assumption of an error for the absolute g–value of ± 0.0001, an agreement to the literature values to within the error was observed. For the time being, until a better way to calibrate the B–axis has been established, for g–values that lie between 2.005 and 2.009, the value of ± 0.0001 will be taken as the measurement uncertainty.

A further consideration has to be made for the determination of relative g–values (g–value differences). For a relative g–value, the error due to the error of the field standard simply cancels. For relative g–values that are determined for lines within the Mn lines, the uncertainty then is the value of ± 0.00002 derived above. For values outside the Mn line range, due to the non–linearity of the error, a general value for the uncertainty cannot be given.

7.1.2 DPPH

A magnetic field standard widely used in EPR experiments is 1,1–diphenyl–2–picryl–hydrazyl free radical (DPPH, figure 7.2). In its solid, polycrystalline form, it exhibits a single EPR line that is narrowed due to Heisenberg spin exchange (figure 7.3).

Previous measurements at mw frequencies of 220 and 250 GHz reported

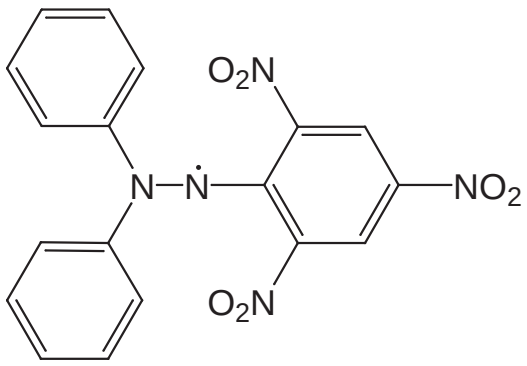

Figure 7.2: Structure of 1,1–diphenyl–2–picryl–hydrazyl (DPPH)

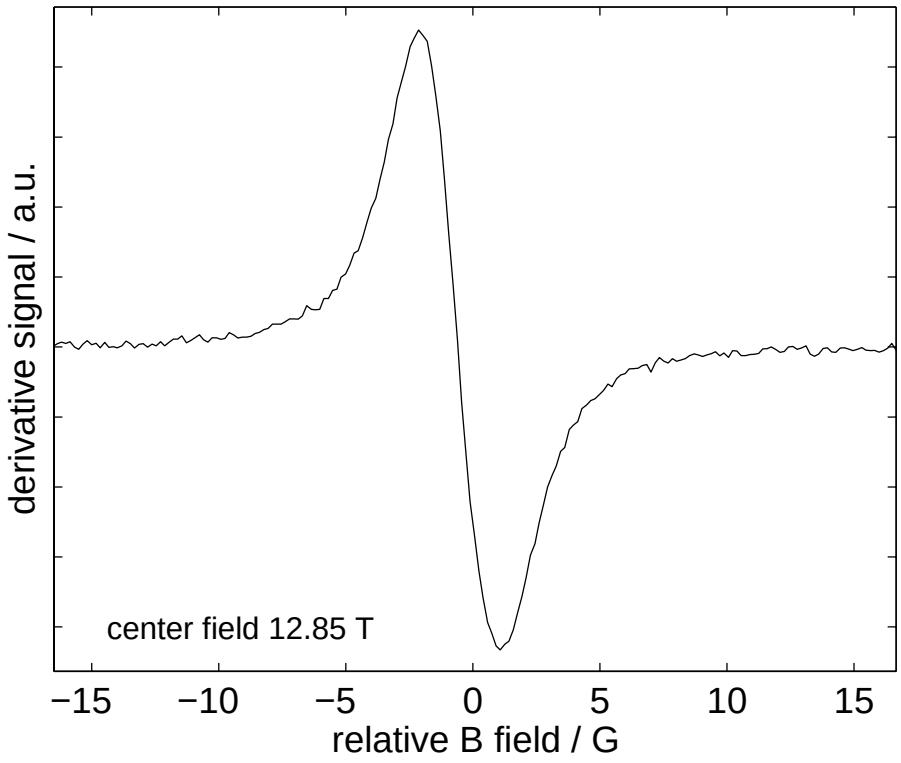

Figure 7.3: EPR spectrum of DPPH polycrystalline powder at room temperature.

a broad structured line (Lynch et al. 1988, Budil et al. 1989, Earle et al. 1996, Cardin et al. 1999). A single, narrow line was reported at 90 GHz by (Smith et al. 1998) and up to 465 GHz by (Krzystek et al. 1997). The variation in linewidth and structure can be ascribed to co–crystallization with the crystallization solvent (Lothe & Eia 1958, Goldsborough et al. 1960, N. D. Yordanov 1996). This has been verified in a later study at 220 GHz (Kolaczkowski et al. 1999); the narrow structureless line was found for samples precipitated from carbondisulfide (CS_2).

This is in accordance with our measurements at 360 GHz; our sample also was recrystallized from CS_2. The peak–to–peak linewidth is 0.3 mT, not significantly broadened when compared to X–band measurements. In our very first measurements with the first probehead, we found that 3 stainless steel

screws fixing the tuning rods to the resonator mirror holder exhibited some residual magnetism. This lead to a broadened line due to field inhomogeneities and was resolved by replacing them with bronze screws. Such a residual field inhomogeneity may also explain the linewidth dependence on the magnetic field observed in (Krzystek et al. 1997).

An isotropic g–value reported in the literature for DPPH is 2.0036 ± 0.0002 (N. D. Yordanov 1996). It was also measured for a polycrystalline powder sample in (K. Möbius 1961) to 2.00366 ± 0.00004. In (Kolaczkowski et al. 1999) a value of 2.00316 ± 0.00002 is quoted.

The Mn^{2+} field standard described in section 7.1, has been measured with similar precision. For an absolute calibration of the magnetic field axis solely based on a standard sample, at least two spectral lines are necessary. This, and considering the g–factor dependence on crystallization solvents reported in (Kolaczkowski et al. 1999), leads to the conclusion that the Mn^{2+} field standard is to be preferred as a field standard for high g–factor resolution measurements.

7.2 Nitroxide radicals

The characteristic structural feature of all nitroxide radicals is the NO group with the nitrogen attached to two alkyl substituents (that often are part of a ring structure; see figure 7.4). They are neutral stable radicals that give rise to the typical powder pattern of a rhombic g–tensor (all principal values g_{ii} different) when measured in the rigid limit. The main spin density of the

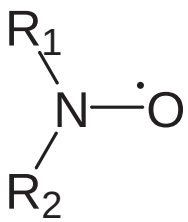

Figure 7.4: General structure of a nitroxide radical. R_1 and R_2 are the alkyl substituents.

unpaired electron is located on the π^* molecular orbital of the NO–bond. The powder pattern therefore also shows a splitting due to the hyperfine tensor of the ^{14}N nucleus.

7.2.1 Sensitivity to solvent polarity

It can be observed that Δg_{xx}, the shift of g_{xx} with respect to the g–value of the free electron g_e,

$$\Delta g_{xx} = g_{xx} - g_e \tag{7.2}$$

reacts strongly to the variation of environmental parameters such as solvent polarity and H–bonds.

This can be understood from the g–factor theory by (A. J. Stone 1963), as laid out in (Burghaus et al. 1993, Prabhananda et al. 1985):

The out–of–plane component of the g tensor of planar hydrocarbon π radicals is equal to the free electron value g_e (i.e. $\Delta g_{zz} = 0$). The in–plane components are generally shifted toward higher values. For the two nitroxide radicals considered in this work, TEMPO and MTSSL, the g–tensor z–axis can therefore be assigned to stand perpendicular to the ring–plane.

It can then be shown that the main contribution to the shifts Δg_{xx} and Δg_{yy} originate from an interaction between the lone–pair orbital in the ring plane on the oxygen and the π^* orbital of the NO–bond.

The lone–pair orbital can be approximated by a linear combination of the s–orbital and the p–orbitals in x– and y–direction

$$\Psi_n^{\mathrm{O}} = c_s s + c_x p_x + c_y p_y \tag{7.3}$$

with the admixture coefficients c_s, c_x and c_y. The g–shifts in x– and y–direction are then given by:

$$\begin{aligned} \Delta g_{xx} &= \frac{2\rho_{\mathrm{O}}^{\pi}\lambda_{\mathrm{O}}c_y^2}{\Delta E_{n\pi^*}} \\ \Delta g_{yy} &= \frac{2\rho_{\mathrm{O}}^{\pi}\lambda_{\mathrm{O}}c_x^2}{\Delta E_{n\pi^*}} \end{aligned} \tag{7.4}$$

with the π spin density on the oxygen, ρ_{O}^{π}, the spin–orbit interaction parameter of the oxygen atom, λ_{O}, and the excitation energy from the lone–pair orbital n to the half–filled π orbital π^*, $\Delta E_{n\pi^*}$.

A change in solvent polarity can then have an effect on Δg_{xx} and Δg_{yy} by shifting the spin density at the oxygen atom, by shifting the excitation energy $\Delta E_{n\pi^*}$ and by varying the admixture coefficients. This has been observed at microwave frequencies of 150 GHz (Ondar et al. 1985) and 250 GHz (Earle et al. 1994). Since $c_y^2 > c_x^2$, the shift of Δg_{xx} exceeds that of Δg_{yy}.

Measurements by (Griffith et al. 1974) have also shown effects of solvent polarity and hydrogen bonding on the z–component of the hyperfine tensor A_{zz} of nitroxide radicals. This can be attributed to a variation of the electron spin density at the nitrogen. For the spin–labeled bacteriorhodopsin that is also measured in the context of this work, polarity–dependent variations of A_{zz} have been observed by (Steinhoff et al. 1999).

7.2.2 g–strain

Mechanisms such as the environment– and orientation–dependent g–tensor components discussed above are the origin of a phenomenon generally called g–strain. g–strain is encountered when an EPR spectrum is broadened not with a homogeneous Lorentzian linewidth due to spin relaxation, but shows an inhomogeneous broadening that is dependent on the static magnetic field B_0.

This dependence on the magnetic field is an indication for the linewidth to be associated with a Zeeman interaction. The broadening is then caused by a distribution in g–values; the origin of the name "g–strain" is that this distribution was ascribed to protein microheterogeneity (Fritz et al. 1971) or hydrostatic stress of the frozen solvent. (W. R. Hagen 1989) and (J. R. Pilbrow 1990) develop a model to simulate EPR spectra that exhibit g–strain broadening by treating the principal values of the g–tensor as random

variables. Spectra that are g–strain broadened can usually only be approximated by a spectral simulation that treats linewidths as a scalar, even when the linewidth is allowed to vary with the anisotropy of the g–tensor. Clearly, a treatment of the g–tensor components as random variables has to make assumptions about a distribution function.

g–strain broadening can be a central problem of high–field EPR measurements. With the apparent linewidth increasing with increasing magnetic field, the spectral resolution enhancement that is one of the main advantages of high–field EPR can be far less than anticipated from a simple consideration of the Hamiltonian terms. As will be indicated in section 7.3, depending on the specific mechanism underlying the observed g–strain broadening the interpretation of the broadening mechanisms can yield additional information about a sample that is not accessible by measurements at lower fields.

7.3 Spectral resolution enhancement

To demonstrate the enhanced resolution achievable by 360 GHz EPR, the spectrum of 4–hydroxy–2,2,6,6–tetramethylpiperidine–1–oxyl free radical (4–hydroxy–TEMPO) was taken at three different magnetic fields B_0 and microwave frequencies f (figure 7.5): $B_0 = 0.34$ T / $f = 9.7$ GHz (X–band), $B_0 = 3.4$ T / $f = 95.6$ GHz (W–band) (A. Savitsky 1999) and $B_0 = 12.8$ T / $f = 360$ GHz.

The solvent in all measurements was a 1:1 water / glycerol frozen solution at 190 K. The sample concentration in the X–band and 360 GHz measurements was 0.8 mM, in the W–band measurements it was 10 mM. The 360 GHz spectrum is an average of 8 scans, recorded with a B–field modulation amplitude of 0.5 mT. The sample was placed in the resonator using the detergent technique as described in section 5.4.

TEMPO is a typical nitroxide radical (section 7.2) with (partly) resolved

hyperfine structure due to the nuclear spin $I = 1$ of the nitrogen ^{14}N (figure 7.6). The hyperfine tensor **A** of the nitrogen is highly anisotropic; with the exact value of A_{zz} dependent on the polarity of the environment, A_{zz} exceeds the value of A_{xx} and A_{yy} by a factor of ~ 6. Also, **A** is an axial tensor ($A_{xx} \approx A_{yy}$); its z–axis is collinear to the z–axis of the **g**–tensor within experimental error (the Euler rotation matrix $R(\phi_A, \theta_A, \psi_A)$ in equation 6.3 can therefore be replaced by the identity matrix in the simulation and fitting routines).

At 360 GHz the isotropic orientation distribution of the solute molecules

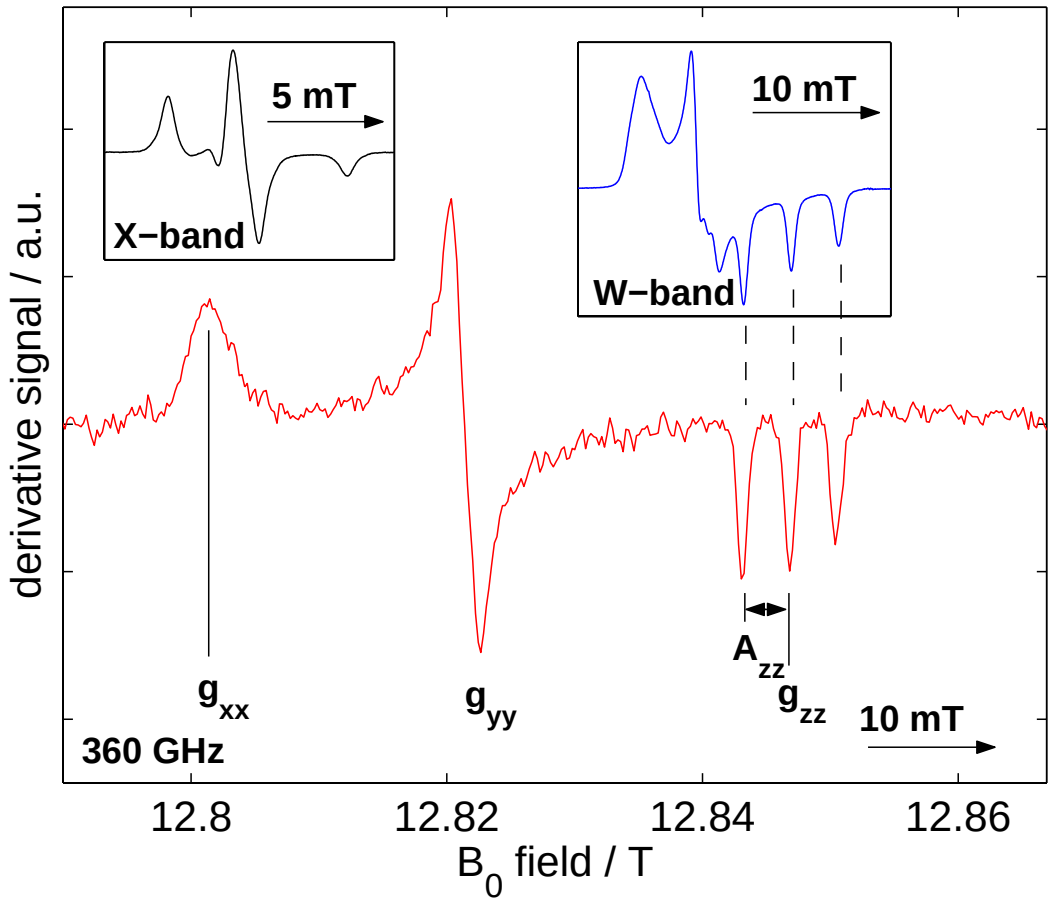

Figure 7.5: 4–hydroxy–TEMPO in water/glycerol ($T = 200$ K) at 360 GHz, 95.6 GHz (A. Savitsky 1999) and 9.7 GHz

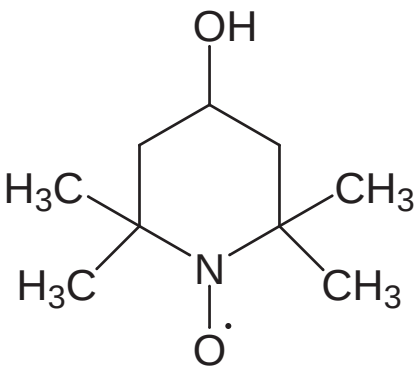

Figure 7.6: Structure of 4–hydroxy–2,2,6,6–tetramethylpiperidine–1–oxyl free radical (TEMPO)

leads to the powder EPR pattern of a rhombic g–tensor system, spread over ~ 50 mT and with the typical turning points associated to the canonical orientations. The z–component of the nitrogen ^{14}N hyperfine tensor A_{zz} causes a splitting of the z–turning point, while the anisotropic g–strain broadening mechanism discussed above (subsection 7.2.2) prevents the line splittings due to the x– and y–components of the hyperfine tensor from being resolved. Clearly, at 360 GHz the Zeeman interaction dominates the spectrum.

For comparison, the inserts in figure 7.5 show the spectra at X– and W–band. At X–band, the hf splitting A_{zz} completely dominates the Zeeman interaction – the anisotropy of the g–tensor can not be resolved at all.

At W–band, hyperfine and Zeeman interaction are still of comparable magnitude. The B–field axis of the W–band and the sub–mm–band spectrum have the same scale; this directly shows the field–independence of the hyperfine splitting (indicated by the dashed lines) and demonstrates that the difference of a factor of 4 in mw frequency directly shows up in the spectral width ($|B(g_{zz}) - B(g_{xx})|$). (The B–field axis scale of the X–band spectrum has been expanded by a factor of 2; the figure insert would become too small otherwise.)

On the basis of the two additional measurements on 4–hydroxy–TEMPO shown in figure 7.7, differences in sample preparation techniques and the different performance of the two probeheads shall be discussed in the fol-

4-hydroxy-TEMPO	g_{xx}	g_{yy}	g_{zz}	A_{zz} / G	Notes
(Ondar et al. 1985)	2.00878	2.00604	2.00215	37.4	**1**
Figure 7.7 top	2.00891	2.00610	2.00221	36.7	**2**

Table 7.1: Spectral parameters of 4–hydroxy–TEMPO; Literature values compared to parameters obtained from the fit in figure 7.7.
Notes: **1** – measurement uncertainty for g_{ii} ± 0.00007, for A_{ii} ±1%, (Ondar et al. 1985) **2** – measurement uncertainty for g_{ii} ± 0.0001, for A_{ii} ± 1 G, see discussion in text

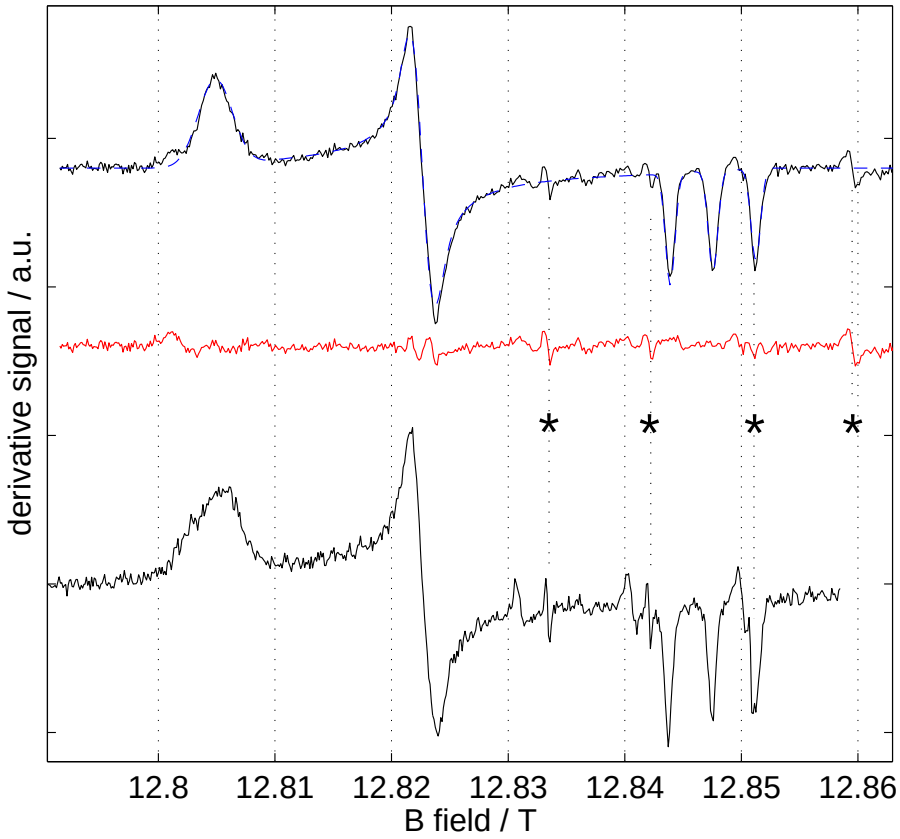

Figure 7.7: 4–hydroxy–TEMPO in water/glycerol ($T = 200$ K) at 360 GHz. The lines marked with the asterisks are the low–field hyperfine transitions of the Mn^{2+} field standard; the broader satellite lines are an artefact (see text). For the labeling of the spectral features, please refer to figure 7.5

lowing paragraphs. The top spectrum has been used to obtain the spectral parameters of 4–hydroxy–TEMPO listed in table 7.1.

The top spectrum in figure 7.7 was acquired using the first probehead configuration (figure 5.5) with a modulation field amplitude of 0.5 mT. The sample concentration was 9 mM, with the sample applied to the resonator mirror by using a cellulose tissue as explained in section 5.4. The trace is the average of 4 single scans; the resonator was retuned after each scan.

Overlayed over the spectrum is the simulation resulting from a least squares fit; the residual is the trace directly below. The **g**– and **A**–tensor components obtained from the fit are listed in table 7.1. The error margins quoted for these values result from the uncertainty in the field calibration. The error margin of 1 G for A_{zz} mainly is caused by the fact that the position of the 3rd line of the Mn field standard coincides with the z–hyperfine component of the spectrum. Within experimental error, the values show satisfactory agreement with the literature values (Ondar et al. 1985).

The spectrum in figure 7.7 at bottom is the first measurement of a resolved **g**–tensor in frozen solution with the new probehead setup (figure 5.6). Here, the sample was placed underneath a curved Mylar sheet (again, see section 5.4). The spectrum shown is an average of 30 separate scans; the resonator was retuned to resonance twice in between. The shoulder exhibited in the g_{xx}–turning point was present in every scan, so an artefact due to field scaling can be ruled out. The broad satellites next to the Mn^{2+} field standard lines appear, because a part of the standard in the polystyrene film was imperfectly sealed and had contact to water. This modifies the crystal structure of the MnO/MgO microcrystalline powder, resulting in the observed broadening.

The main result from the comparison between the two measurements is the fact that the resonator behaved much more stable in the new configuration. With all other conditions as far as the probehead is concerned equal, the drifting of the resonator mode – caused mainly by the vibrations due to

the microphonic effects of the field modulation – was much reduced. This allowed to take much more scans without retuning the resonator.

The sample placement using a Mylar sheet, however, proved somewhat problematic. Compared to the top spectrum, it was not possible to achieve as good coupling, resulting in a lower B_1 microwave field at the sample and thus in a lower signal–to–noise ratio. Also, the Mylar sheet is very susceptible to static charges. The asymmetric broadening of the g_{xx} turning point in the bottom spectrum could be attributed to a non–isotropic environment, causing a shift in the g_{xx}–values for a subensemble of the molecules in the sample. This effect would be very similar to the shift–mechanism described in subsection 7.2.1. Obviously, further studies are neccessary to fully understand this effect.

The above example clearly is a case where an interpretation of the spectrum is not feasible, since the spectral features are influenced by interactions with the environment, rather than being representative for the molecule under observation. At lower fields this effect might easily go unnoticed, however, and a fit to the spectrum would yield an average value of g_{xx} that is not related to internal properties of the sample.

7.4 Spin–labeled proteins: bacteriorhodopsin

In the context of a research program focused on high–field EPR (Deutsche Forschungsgemeinschaft 1997), measurements on spin-labeled bacteriorhodopsin (bR) have been performed in W–band in our workgroup (Savitsky et al. 1999). One of those samples was chosen for a first measurement of a biologically relevant protein with the typical low spin–concentrations. This ensured that experimental data for comparison was readily available from the W–band measurements. In the following paragraphs, a brief description of the functioning principles of bR will be given.

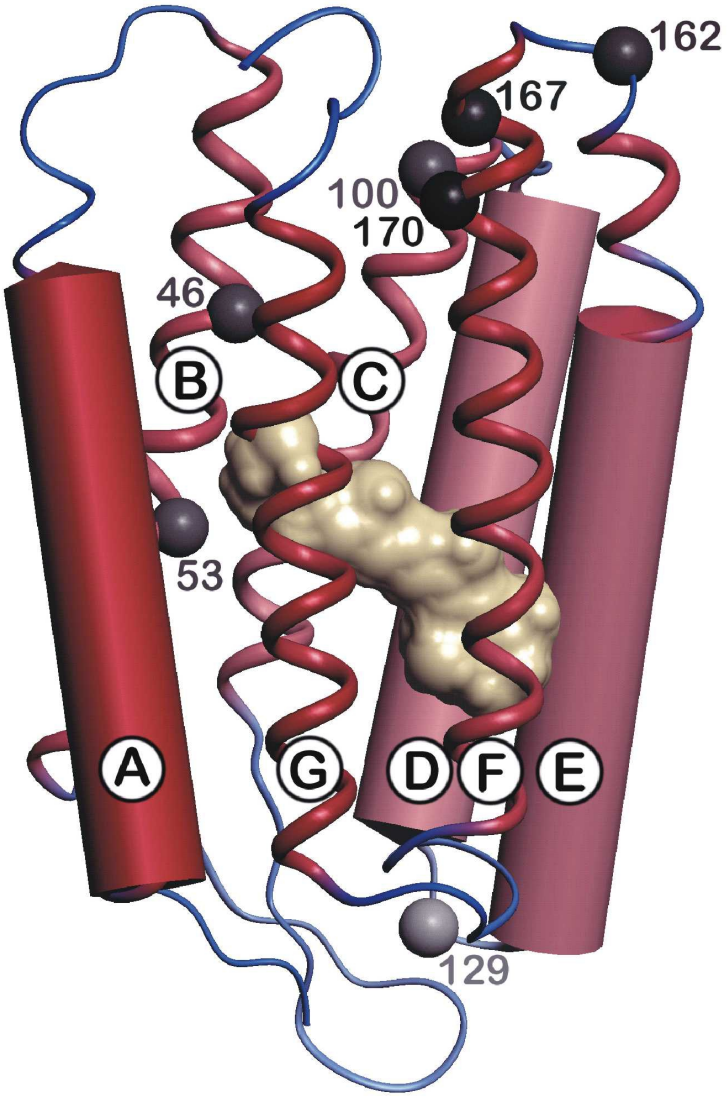

Figure 7.8: Structure of bacteriorhodopsin; the helices along the proton transport channel are marked A through G, the amino acids that were spin labeled in the course of the work of (Steinhoff et al. 1999) are marked with their sequence number. The sample measured in this work was labeled at position 167, close to the cell interior (top of figure). The extracellular end is at the bottom of the figure (Figure courtesy of A. Savitsky and H.J. Steinhoff, 1999.)

Bacteriorhodopsin (figure 7.8) is an ion transport protein found in halo bacteria. It absorbs light and uses the energy to establish a proton gradi-

ent across the cell membrane that is subsequently used for ATP (adenosine triphosphate) production. bR has become a paradigm for membrane and transport proteins and its structure has been determined by X–ray crystallographic studies and electron diffraction methods, among others. A recent comprehensive review can be found in (Haupts et al. 1999).

As far as EPR is concerned, a technique that has been very successful in gaining structural and functional insight into the processes governing bR has been that of spin labeling. By means of the biochemical technique of site–directed mutagenesis (figure 7.9), such spin labels can be covalently bound to precisely defined locations in the amino acid chain of the protein (Hubbell & Altenbach 1994). The sensitivity of the spin label EPR spectra to differ-

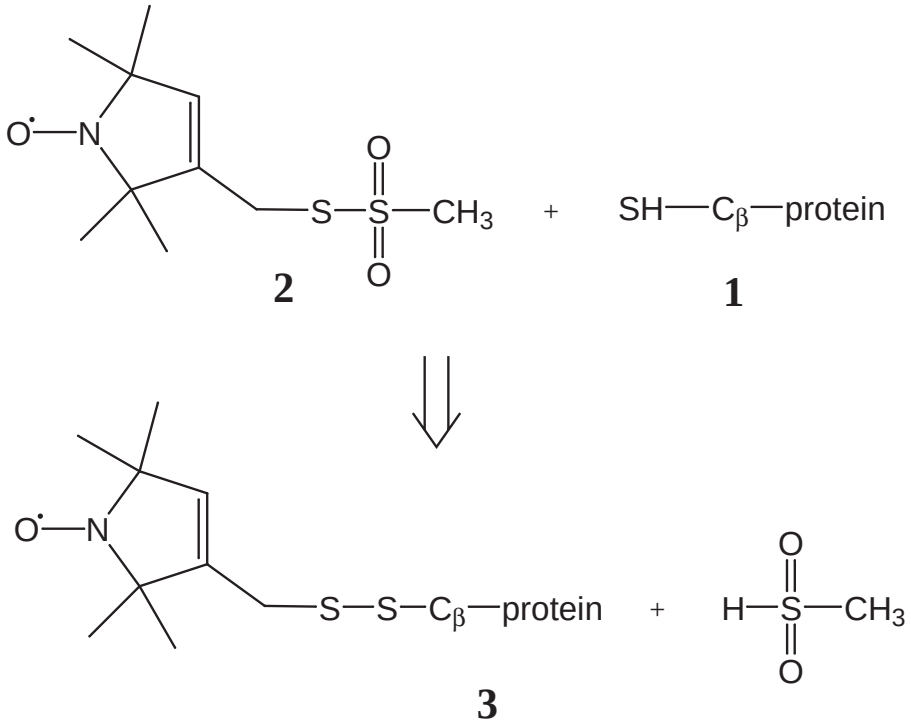

Figure 7.9: MTSSL spin label and site–directed mutagenesis: In the protein to be labeled, a specific amino–acid is replaced via mutation by a cysteine (**1**). To this cysteine, a (1–oxyl–2,2,5,5–tetramethylpyrroline–3–methyl)methanethiosulfonate spin label (MTSSL, **2**) can be covalently attached (**3**).

ent environments inside the protein structure (polarity, mobility) provides information about parameters not easily obtainable otherwise.

The spin label employed in the present study was (1–oxyl–2,2,5,5–tetramethylpyrroline–3–methyl)methanethiosulfonate spin label (MTSSL, figure 7.9, **2**). Albeit being invasive, provided this procedure does not critically interfere with the function of the protein, it enables one to study biological processes in an environment more closely resembling physiological conditions than using e.g. X–ray diffraction methods.

The focus of the current W–band measurements was to determine the polarity profile along the proton transport channel. This channel is formed by seven transmembrane helices, labeled A to G in figure 7.8. As laid out in subsection 7.2.1, the hyperfine and **g**–tensor components A_{zz} and g_{xx} of nitroxide spin labels are sensitive to the polarity of their environment. By attaching spin labels to different amino acids along the channel, a profile of the hydrophobic barrier can be obtained (Steinhoff et al. 1999).

The sample under investigation in the 360 GHz EPR measurements presented here is the mutant V167C (amino–acid valine at position 167 exchanged against cysteine). The point of mutation is located at the cytoplasmic (cell–interior) end of the proton channel (figure 7.8), a position in which a higher environment polarity is expected compared to the interior of the channel.

As will become clear below, this choice of mutant would be very impractical if the scope of the measurement presented here was the actual measurement of the polarity profile as in the W–band measurements. The V167C mutant actually shows one of the smallest shifts in g_{xx}–values compared to the free spin label. Instead, the choice rather was dictated by the sufficient availability of the sample. This is because in contrast to the W–band measurements, where the sample can remain in a sealed tube for the course of the experiment and therefore be reused, in the current setup at 360 GHz the

sample can be measured only once.

The spectrum of the spin–labeled bR mutant was compared to a standard spectrum – that of the free spin–label MTSSL. The solvent in both cases was a 1:1 water / glycerol mixture. The concentration of MTSSL spin label was $\sim$ 1 mM, that of bR 0.2 mM. Both samples were applied to the mirror with the glucopyranoside detergent technique described in section 5.4. The field modulation amplitude was 5 G. Both spectra were fitted with the simulation routine described in chapter 6. The g_{xx}–region in the two spectra does not exhibit asymmetric broadening as observed in the TEMPO measurement in figure 7.7 at bottom. The approach to fit the spectra with the empirical model of orientation–dependent linewidths therefore is justified.

The values for g_{xx} obtained from the fit to the MTSSL spectrum show a small shift to smaller values (table 7.2 and table 7.3). This is what would be expected for a higher environment polarity. With the spin label position of the V167C mutant being close to the membrane surface, the polarity of its environment is higher than in the membrane interior; the shift of its g_{xx}–value with respect to that of MTSSL therefore is expected to be minimal. Considering the measurement uncertainty of the g_{xx}–value of ± 0.0001 due to the uncertainty in the field calibration, the shift actually is not significant within experimental error. This is also the case for the hyperfine tensor

MTSSL	g_{xx}	g_{yy}	g_{zz}	A_{zz}	Notes
(Bennati et al. 1999)	2.00848	2.00610	2.00217	36.1	**1**
(A. Savitsky 1999)	2.00834			36.4 $\pm$ 0.2	**2**
Figure 7.10	2.00856	2.00605	2.00222	36.0	**3**

Table 7.2: Magnetic parameters of MTS spin label; Literature values compared to parameters obtained from the fit in figure 7.10 bottom.
Notes: **1** – measurement uncertainty for $g_{ii} \pm 0.00005$, not given for A_{ii} (Bennati et al. 1999). **2** – possible shift of absolute g–value; irrelevant for measurement of relative shifts **3** – measurement uncertainty for $g_{ii} \pm 0.0001$, for $A_{ii} \pm 1$ G, see discussion in text

bR	g_{xx}	g_{yy}	g_{zz}	A_{zz} / G	Notes
(Savitsky et al. 1999)	2.00849			36.3	**1**
Figure 7.10	2.00862	2.00607	2.00225	37.1	**2**

Table 7.3: Magnetic parameters of spin labeled bacteriorhodopsin mutant V167C; Values measured in W–band (A. Savitsky 1999) compared to parameters obtained from a fit to the spectrum in figure 7.10, top.
Notes: **1** – possible shift of absolute g–value; irrelevant for measurement of relative shifts **2** – measurement uncertainty for $g_{ii} \pm 0.0001$, for $A_{ii} \pm 1$ G, see discussion in text

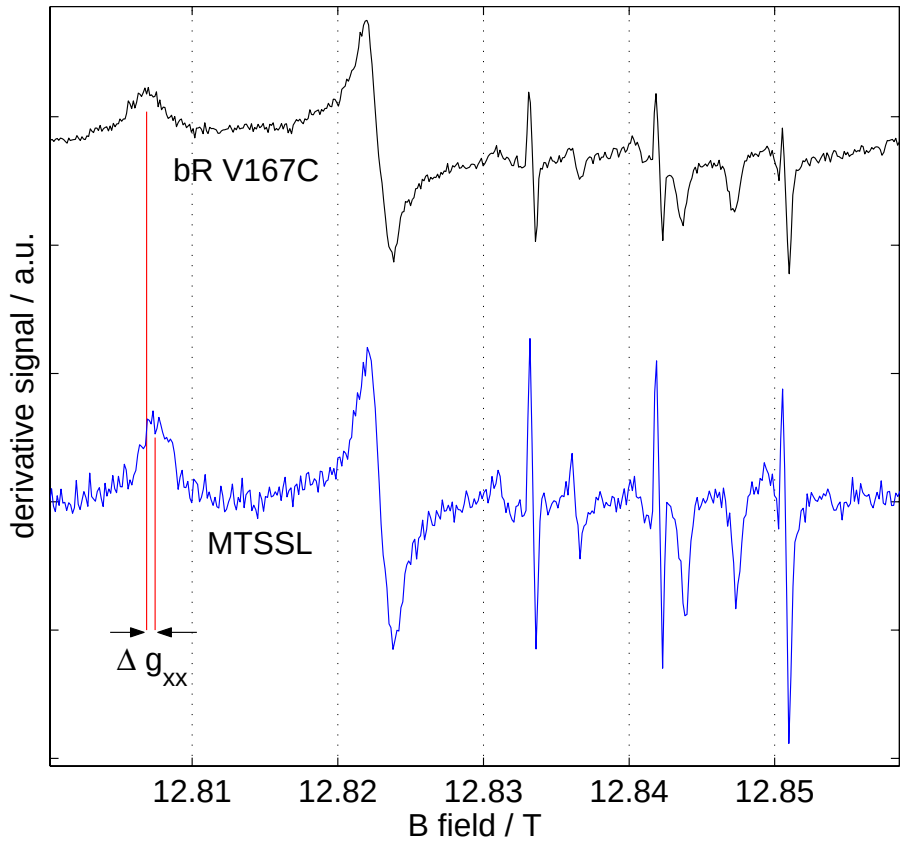

Figure 7.10: Comparison of the 360 GHz EPR spectra of the spin–labeled mutant V167C and of a solution of the free spin–label MTSSL at $T = 190$ K. For the labeling of the spectral features, please refer to figure 7.5

component A_{zz}.

The comparison with the absolute g–values obtained in W–band should solely consider the relative shifts of g_{xx} between MTSSL and the bR mutant. These are in good agreement. The absolute g–values of the W–band measurement could be systematically shifted due to a slightly different position of sample and standard (A. Savitsky 1999). For the purpose of determining relative g–values for the various bR mutants, this shift is irrelevant.

It should be stressed here, that the achievement must be seen in the fact that the bacteriorhodopsin mutant with its low spin concentration could be measured at sufficiently high signal–to–noise to allow for extraction of the relevant spectral parameters. The main objective when considering further measurements of spin labels or other nitroxide radicals at 360 GHz clearly is to improve the field calibration routine to minimize the error margin of the g–value measurements.